A shelf-life study of silica- and carbon-based mesoporous materials

Journal of Industrial and Engineering Chemistry 101 (2021) 205–213

Contents lists available at ScienceDirect

Journal of Industrial and Engineering Chemistry

journal homepage: www.elsevier.com/locate/jiec

A shelf-life study of silica- and carbon-based mesoporous materials

Emma M. Björk [a,b,*], Aylin Atakan [a,b], Pei-Hsuan Wu [b], Alessandra Bari [c], Carlotta Pontremoli [c], Kai Zheng [d], Dimitra Giasafaki [e], Giorgio Iviglia [f], Elisa Torre [f], Clara Cassinelli [f], Marco Morra [f], Theodore Steriotis [e], Georgia Charalambopoulou [e], Aldo R. Boccaccini [d], Sonia Fiorilli [c], Chiara Vitale-Brovarone [c], Fredrik Robertsson [b], Magnus Odén [a,b]

[a] Nanostructured Materials, Dept. of Physics, Chemistry and Biology, Linköping University, 581 83 Linköping, Sweden
[b] Nanolith Sverige AB, Ferievägen 15, 168 41 Bromma, Sweden
[c] Department of Applied Science and Technology, Politecnico di Torino, Corso Duca degli Abruzzi 24, 10129 Torino, Italy
[d] Institute of Biomaterials, University of Erlangen-Nuemberg, 91058 Erlangen, Germany
[e] National Centre for Scientific Research "Demokritos", Agia Paraskevi Attikis, 15341 Athens, Greece
[f] Nobil Bio Ricerche srl, Via Valcastellana 26, 14037 Portacomaro (Asti), Italy

ARTICLE INFO

Article history:
Received 16 April 2021
Revised 4 June 2021
Accepted 13 June 2021
Available online 18 June 2021

Keywords:
Mesoporous bioactive glass
Mesoporous silica
Mesoporous carbon
Materials stability
Shelf-life

ABSTRACT

Mesoporous silica- and carbon-based materials, including bioactive glasses, have proven potential as components of medical devices and as drug carriers. From an application perspective, knowledge about the shelf-life stability of these materials under various conditions is vital. Here, mesoporous bioactive glasses (MBGs) synthesized by aerosol-assisted spray-drying and by a batch sol–gel method, mesoporous silicas of SBA-15 type, and mesoporous carbons CMK-1 and CMK-3 have been stored under varying conditions, e.g. at different temperature and relative humidity (RH), and in different storage vessels. The results show that the silica-based materials stored in Eppendorfs are sensitive to humidity. Spray dried MBGs decompose within 1 month at a RH >5%, whilst sol–gel MBGs are more stable up to a RH >60%. Changing the storage vessel to sealed glass flasks increases the MBGs lifetime significantly, with no degradation during 2 months of storage at a RH = 75%. SBA-15 stored in Eppendorfs are more stable compared to MBGs, and addition of F^- ions added during the synthesis affects the material degradation rate. Mesoporous carbons are stable under all conditions for all time points. This systematic study clearly demonstrates the importance of storage conditions for mesoporous materials which is crucial knowledge for commercialization of these materials.

Introduction

Mesoporous silica- and carbon-based materials have during the last 25 years gained significant interest as drug delivery systems. Due to their large specific surface area, pore size of 2–15 nm, and controllable composition, these materials can be tailored to be loaded with both hydrophilic and hydrophobic drugs enabling a targeted delivery. Mesoporous bioactive glasses (MBGs) have proven to have significant osteogenic properties due to their ability to bind to bone through the formation of carbonated hydroxyapatite [1,2]. In addition, thanks to the possibility to incorporate and release specific therapeutic ions such as strontium which is pro-osteogenic, the bone regeneration is further enhanced [3]. Addition of other ions, e.g. Cu (pro-angiogenic and antibacterial) [4–6] or Ce (pro-angiogenic and anti-inflammatory) [7], enables the exploitation of this materials family for wound healing applications [8]. MBGs used for medical applications can be synthesized through several procedures, including 3D printing for producing scaffolds [9], as well as spray-drying [10,11] and sol–gel methods [5,12,13] for particle synthesis allowing particles with variable sizes and pore characteristics. Mesoporous silica and carbon particles have also attracted interest as drug delivery systems [14,15]. Monodispersed mesoporous silica particles of SBA-15 type have shown potential in both drug delivery and enzyme immobilization [16,17], and can be synthesized with various morphologies and porosities [18]. By functionalization with organics and metals, mesoporous silica, such as SBA-15, can be used both in heterogeneous catalysis [19–26], photocatalysis [27], and sensing [28,29]. On the other hand, mesoporous carbons have been shown to bring

* Corresponding author.
E-mail address: emma.bjork@liu.se (E.M. Björk).

https://doi.org/10.1016/j.jiec.2021.06.011
1226-086X/

significant advantages in e.g. chemotherapy, bio-detection and real-time imaging due to e.g. their inertness, biocompatibility and high loading capacity [30]. In addition, decorating the mesoporous carbons with Ag nanoparticles makes them useful also in healing of chronic wounds [31], and the addition of a pH-responsive polymer layer enables a controlled release of the nanoconfined cargo [32].

From a commercialization perspective, and also for handling in a research lab, it is crucial to demonstrate the stability of the mentioned materials during storage. Mesoporous silicas of e.g. MCM-41, MCM-48 and SBA-15 types, and mesoporous carbons without therapeutic ions are commercially available today, but materials functionalized with ions are not possible to purchase. Material degradation in vitro and in vivo has been extensively investigated for both MBGs and mesoporous silicas. However, there are only a few studies on the shelf-life stability of mesoporous materials, and none of them compare mesoporous materials with various chemical compositions or synthesis methods. Menci et al. recently reported that bioactive glass-based glass–ceramic scaffolds are sensitive to an atmosphere containing both humidity and CO_2, which caused formation of carbonates and hydrocarbonates [33]. Adeniran and Mokaya stored mesoporous silica of MCM-41 type for 12 years on an open benchtop in conventional sample vials and compared its properties with freshly synthesized materials [34]. They observed that the hydrothermal treatment temperature during the material synthesis affected the shelf-life stability, and that the as-synthesized samples presented high stability and characteristics similar to the freshly prepared samples after 12 years of storage. However, a systematic study of the shelf-life of MBGs, mesoporous silica, or mesoporous carbons in controlled environments has not been reported previously.

The aim of this study is to investigate the possible structural alteration of mesoporous silica- and carbon-based materials such as MBGs with therapeutic ions (copper, strontium, and cerium), mesoporous silicas of SBA-15 type, and mesoporous carbons of CMK-1 and CMK-3 types upon storage. The final goal is to find the optimum long-time storage conditions for these materials and provide information on suitable material handling when working with these materials. Emphasis was placed on monitoring the evolution of key features of the respective particles (such as surface area, porosity, and particle morphology) after their packing, sterilization, and storage in different conditions. All silica-based materials were stored both with and without micelles in the pores. In the case of MBGs, the materials showing the most pronounced degradation upon storage in Eppendorfs, the effects of changing the storing vessel to glass vials were investigated. The sterility, cytotoxicity, and ion release profiles of materials stored in glass vials were examined in addition to the structural stability investigation. The derived information is of importance for industrial applications of these materials families.

Experimental

Synthesis

MBGs

Spray-drying procedure of MBG with Sr. The spray drying synthesis was performed following the protocol reported by Fiorilli et al. [3]. Briefly, 2.03 g of P123 was dissolved in 85 g of double distilled water. In another beaker, 10.73 g of TEOS was pre-hydrolysed under acidic conditions using 5 g of HCl solution (pH 2) until a transparent solution was obtained. The TEOS-containing solution was added dropwise to the micellar solution and was stirred for 1 h. Then, 1.86 g of $Ca(NO_3)_2{\cdot}4H_2O$ and 0.32 g $SrCl_2$ were added to the mixture. The final solution was stirred for 15 min and then sprayed with a Büchi, Mini Spray-Dryer B-290 using nitrogen as the atomizing gas with the following parameters: inlet temperature 220 °C, N_2 pressure 60 mmHg and feed rate 5 mL/min. The obtained powder was finally calcined at 600 °C in air for 5 h at a heating rate of 1 °C/min using a Carbolite 1300 CWF 15/5. The material is labelled MBG_SD_Sr.

Sol-gel synthesis of MBGs with Sr or Cu. MBGs containing strontium and copper were prepared using a base-catalysed template sol–gel synthesis, based on a procedure reported by Pontremoli and Boffito et al. [10,35]. Briefly, 6.6 g cetyltrimethylammonium bromide (CTAB) and 12 mL of ammonium hydroxide were dissolved in 600 mL of distilled water under magnetic stirring for 30 min at 350 rpm. Then, 30 mL of tetraethyl orthosilicate (TEOS), 4.88 g calcium nitrate tetrahydrate and ion precursor (0.86 g of $SrCl_2{\cdot}6H_2O$ or 0.43 g of $CuCl_2$) were added and kept under vigorous stirring for 3 h.

The materials were collected by centrifugation, washed once with distilled water and twice with absolute ethanol. The final precipitate was dried at 70 °C for 12 h and then calcined at 600 °C in air for 5 h at a heating rate of 1 °C/min. The materials are named MBG_SG_Sr and MBG_SG_Cu.

Sol-gel synthesis of MBGs with Ce. MBGs containing cerium were synthesized using a microemulsion-assisted sol–gel method from Zheng et al. [4,7]. Briefly, 0.7 g of CTAB was dissolved in 33 mL of deionized water under continuous stirring before the addition of 10 mL of ethyl acetate. After stirring for 30 min, 7 mL of aqueous ammonia (1 M) was added with a further 15 min of stirring. 3.6 mL of TEOS and 2.28 g of calcium nitrate tetrahydrate were then sequentially added with an interval of 30 min. The resulting mixture was then stirred for an additional 4 h. The formed nanoparticles were collected by centrifugation and washed twice with deionized water and once with ethanol (96%). The collected particles were then dried at 60 °C overnight prior to calcination at 700 °C for 3 h with a heating rate of 2 °C/min. This material is named MBG_SG_Ce_Parent.

To incorporate Ce into the MBGs, an adapted post-impregnation method was performed following the route from Kozon et al. [36]. Briefly, MBG_SG_Ce_Parent were soaked in an ethanol solution of cerium nitrate (0.2 M) at the concentration of 10 mg/mL under stirring for 24 h at 20 °C. After the impregnation process, the treated MBG were washed with ethanol twice before drying at 60 °C overnight. The dried nanoparticles were then calcined at 680 °C for 2 h with a heating rate of 2 °C/min. This material is named MBG_SG_Ce.

Mesoporous silicas of SBA-15 type

Mesoporous silica of SBA-15 type was synthesized following the protocol from Björk et al. [18]. Briefly, 4.8 g of triblock copolymer $EO_{20}PO_{70}EO_{20}$ (Pluronic P123) and either 0 or 56 mg of NH_4F were dissolved in 160 mL of 1.84 M HCl under vigorous stirring at 20 °C. 2 or 8 mL of heptane and 11 mL of TEOS were premixed and added to the micelle solution. The mixture was stirred for 4 min and then kept under static conditions at 20 °C, overnight. The mixture was transferred to PTFE bottles for hydrothermal treatment in an oven at 100 °C for 24 h. The materials were collected by filtration,

Table 1
Additives used during the synthesis of the different SBA-15 materials.

Material	Heptane/P123 molar ratio	NH_4F/P123 molar ratio
SBA-15_1	16	0
SBA-15_2	16	1.8
SBA-15_3	64	1.8

washed with deionized water, and finally calcined at 550 °C for 5 h with a heating rate of 1 °C/min. The different SBA-15 materials obtained are listed in Table 1.

Mesoporous carbons

CMK-1 with Ag. CMK-1 carbon spheres were prepared using sucrose as the carbon precursor and cubic periodic silica MCM-48 spheres as the starting hard template, following a previous reported procedure [32]. Based on a modified Stöber method [37], the silica spheres were prepared by using a mixture of two different surfactants (CTAB and triblock copolymer $EO_{106}PO_{70}EO_{106}$–Pluronic F127) and TEOS 98% as the silica source at a composition of 1:4:3.6 g in 298 mL of an ethanol:aqueous ammonium hydroxide 2.8 wt% solution of 1:2.5 (v/v) at ambient temperature [38]. The resulting silica was obtained after thorough washing, centrifugation and drying at 40 °C in air, followed by calcination at 550 °C for 6 h under air flow.

The calcined MCM-48 was impregnated twice with acidic sucrose solution, consisting of 1.25 g of sucrose in a mixture of 5 g of water and 8 drops of H_2SO_4 the first time and of approx. 65% of the sucrose the second time. The carbon with the inverse structure and the spherical morphology (CMK-1) was obtained by dissolving the silica with hydrofluoric acid (HF) after the thermopolymerization of the impregnated template, each time at 100 °C and 160 °C for 6 h, and the carbonization of the final composite at 900 °C for at least 2 h under N_2 gas flow [32,39].

The CMK-1 carbon spheres were decorated with 2 wt% of Ag^0 nanoparticles using $AgNO_3$ as metal source and high grade $NaBH_4$ as reducing agent. 2 g of CMK-1, produced as described above, were dispersed into deionized water, followed by the dropwise addition of an aqueous solution of $AgNO_3$, corresponding to 2 wt % of Ag on the mesoporous carbon. The mixture was kept in the dark for 24 h whilst stirring at room temperature. Subsequently, an aqueous solution of $NaBH_4$ (in excess) was added dropwise and kept under stirring for 1 h before filtration. The obtained solid was washed with distilled water and acetone and dried at 40 °C.

CMK-3 with Ag. CMK-3 was synthesized starting from the hexagonally ordered mesoporous silica SBA-15 using the standard hard-templating approach [40]. The latter was prepared according to a typical method under aqueous acidic conditions [41], using triblock copolymer $EO_{20}PO_{70}EO_{20}$ (Pluronic P123) as surfactant, and TEOS 98% as silica source at a ratio of 1 g P123:2 g of TEOS in 38 mL HCl 1.6 M. The hydrothermal reaction took place in an autoclave at 35 °C for 20 h and the aging process at 90 °C for 24 h [32].

CMK-3 was obtained by impregnation of the SBA-15 twice with acidic sucrose solution (similarly to the CMK-1 case described above), followed by polymerization at 100 °C and 160 °C for 6 h each time and finally carbonization at 900 °C for at least 2 h under N_2 gas flow [32,39]. The silica framework was removed using HF at room temperature.

The CMK-3 was decorated with 2 wt% of Ag^0 nanoparticles following the same protocol described above for the case of CMK-1.

Packing, sterilization and storage

In the initial study, ~0.2 g of particles of all material types were packed in Eppendorfs, which were closed and sealed with parafilm. In the case of the silica-based materials, both calcined and uncalcined particles were investigated; the amount of uncalcined particles was adjusted so that it would yield ~0.2 g of material after calcination. The materials calcined after storage were calcined using the same conditions as described above. The Eppendorfs were placed in cardboard boxes and sterilized using 25 kGy gamma radiation prior to storage in controlled environments. The storage conditions were:

- Accelerated: 40 °C and 75 % relative humidity.
- Room: 25 °C and 60 % relative humidity.
- Dry: 25 °C and <5 % relative humidity.

The materials were stored in Eppendorfs for 6 months in accelerated conditions, and 12 months in room and dry conditions.

In the second study, two selected materials, MBG_SG_Cu and MBG_SD_Sr, were packed in glass vials sealed with rubber seal caps and a plastic cap. The packed materials were sterilized using 25 kGy gamma radiation prior to storage in accelerated conditions (40 °C and 75 % relative humidity) for 2 months.

Materials characterization

The materials morphology was observed using a LEO (Zeiss) 1550 Gemini scanning electron microscope (SEM) operated at 3 kV. The atomic composition of the materials was determined by X-ray energy dispersive spectroscopy (EDS) using an Oxford X_Max 80 system attached to the SEM and operated at 20 kV. Pore characteristics were determined by nitrogen physisorption measurements at 77 K using a Micromeritics ASAP 2020. The materials were degassed at 200 °C for 6 h prior to the analysis. The Brunauer–Emmett–Teller (BET) area values were calculated at a pressure range of P/P_0 = 0.08–0.18, and the total pore volume was determined at P/P_0 = 0.99. The pore size distributions (PSDs) were calculated from the adsorption branches of the isotherms by using the KJS (Kruk-Jaroniec-Sayari) method. The physisorption data is presented in the supplementary information (Tables S1–S14, and Figs. S1–S14).

Ion release

In order to evaluate the concentration of released ions, the MBG_SG_Cu and MBG_SD_Sr were soaked in Tris HCl buffer (0.1 M, pH 7.4) with a concentration of 250 μg/mL, according to the protocol described by Shi et al. [42]. Briefly, 5 mg of powder were suspended in 20 mL of buffer up to 14 days at 37 °C in an orbital shaker (Excella E24, Eppendorf) with an agitation rate of 150 rpm. At defined time points (3 h, 24 h, 3 days, 7 days and 14 days) the suspension was centrifugated at 10,000 rpm for 5 min (Hermle Labortechnik Z326, Wehingen, Germany). Half of the supernatant was collected and replaced by the same volume of fresh buffer solution to keep the volume of the release medium constant. The release experiments were carried out in triplicate and results have been reported as mean ± standard deviation. The ion content was measured by Inductively Coupled Plasma Atomic Emission Spectrometry Technique (ICP-AES) (ICP-MS, Thermoscientific, Waltham, MA, USA, ICAP Q), after appropriate dilutions.

Sterility and cytotoxicity

The sterility test was performed on MBG_SD_Sr and MBG_SG_Cu by using a Gram-positive *Staphylococcus epidermidis* RP62A (ATCC 35984) bacterial strain. The strain was routinely kept in Tryptic Soy Agar (TSA, Sigma). The test was performed by transferring 5 mL of Tryptic Soy Broth (TSB, Sigma) in a 15 mL falcon tube with 1 mg of MBGs and left at 37 °C for 72 h and at room temperature for other 72 h. The positive control was obtained using 5 mL of TSB with 10 μL of bacterial suspension (*S. epidermidis*). As negative control, 5 mL of TSB was used. The contamination was determined by evaluation of the transparency of the TSB solution; the cloudiness of the solution denotes bacterial contamination of the material.

Cell viability tests were performed using a 3-(4,5-Dimethylthiazol-2-yl)-2,5-diphenyltetrazolium bromide (MTT) assay with L929

fibroblast cells. The cells were seeded on a polystyrene plate and 1 mg of MBG_SD_Sr and MBG_SG_Cu were added, and the cell viability was evaluated after 72 h of incubation. The test allows assessment of the possible toxic effect of particle dissolution products on cells, by evaluating the reduction of the mitochondrial succinate dehydrogenase (SDH) enzyme activity, normally involved in the citric acid cycle. A preliminary qualitative assessment was carried out through inverted microscope (LEICA DMI4000B, Leica Microsystems, Wetzlar, Germany). Optical images of the cells in direct contact with MBG_SD_Sr and MBG_SG_Cu particles are presented with a scale bar of 100 μm. In the MTT test, the cells were incubated with a 1 mg/mL solution of soluble tetrazolium salt (3-(4,5-dimethylthiazol–2yl)-2,5 diphenyl tetrazolium bromide). During the subsequent two hours of incubation at 37 °C, the succinate dehydrogenase enzyme causes the transformation of tetrazolium salts into a yellow soluble substance first and then into a blue water-insoluble product, the formazan precipitate. From the quantification of the precipitate product, it is possible to evaluate the degree of the enzyme activity and, consequently, the number of metabolically active cells. To perform this evaluation, the formazan precipitate was dissolved with dimethylsulphoxide and was spectrophotometrically measured at a wavelength of 570 nm, providing an optical density (OD) value. Cells grown on polystyrene plate were used as negative control, while cells grown with the addition of 20 μL of a solution of 0.08 mg/mL of Sodium nitroprusside (NPS) were used as the positive control. The data is presented relative to the negative control.

Results and discussion

Storage in Eppendorfs

MBGs stored in Eppendorfs

The materials' stability was studied by nitrogen physisorption measurements at 77 K, SEM and EDX. Fig. 1 shows the evolution of the specific surface area and total pore volume for the MBGs: MBG_SD_Sr, MBG_SG_Sr, and MBG_SG_Ce stored at three different conditions, and with and without micelles (i.e. prior to and after calcination). In general, it is observed that the MBGs degrade fastest when stored under accelerated conditions and are most stable in dry conditions. Also, the materials calcined after storage, i.e. stored with micelles in the pores, keep their specific surface area and total pore volume to a larger extent compared to materials calcined prior to storage.

Despite the apparent changes in the pore structure of the MBG materials, no substantial morphological changes can be observed upon storage. For example, the SEM micrographs in Fig. 2 show the morphology of the MBGs prior to storage (left) and after storage under accelerated conditions for six months (right). All MBGs retain their spherical morphology during storage, although accelerated storage conditions (40 °C and 75 % relative humidity) for 6 months clearly have the largest effect on their pore characteristics. MBG_SD_Sr (Fig. 2(a, b)) show a broad particle size distribution between 1 – 3 μm, MBG_SG_Sr (Fig. 2(c, d)) particles have a diameter of 80 – 100 nm, and the mean size of MBG_SG_Ce (Fig. 2(e, f)) particles is ~130 nm. The particle sizes before and after storage in accelerated conditions are presented in the supplementary information, Table SI 15. The difference in morphology between the different synthesis methods are due to differences in the material formation route. The sol–gel synthesized materials have a narrow particle size distribution due to the slow particle formation rate where the siliceous network is formed around CTAB micelles, whilst the larger particles formed by spray drying are affected by the nozzle pressure and fast solvent evaporation during the spraying [43]. Despite the difference in particle morphology, all

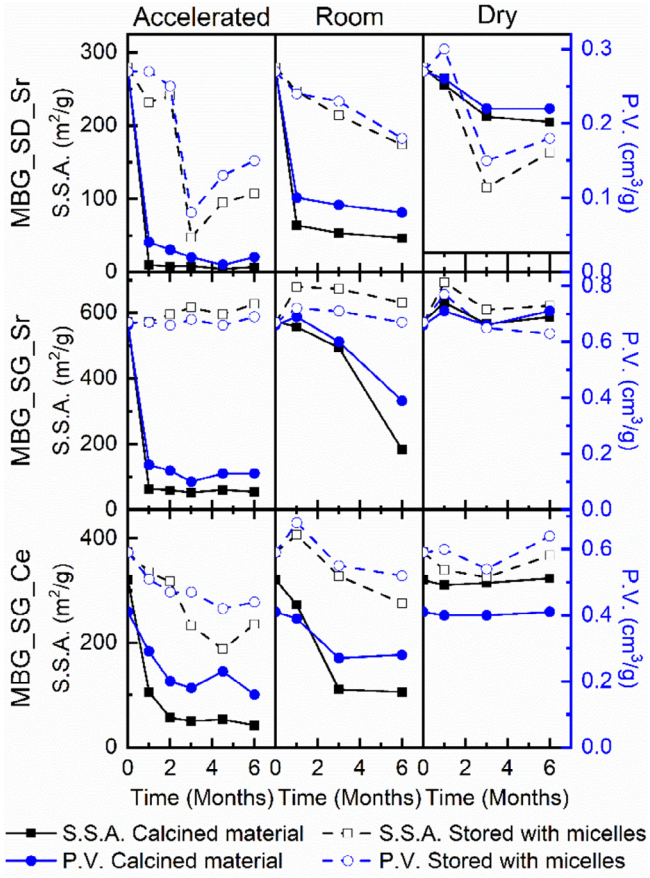

Fig. 1. Evolution of specific surface area and total pore volume for MBG_SD_Sr stored with and without micelles, MBG_SG_Sr stored with and without micelles, and MBG_SG_Ce stored without micelles and MBG_SG_Ce_Parent stored with micelles.

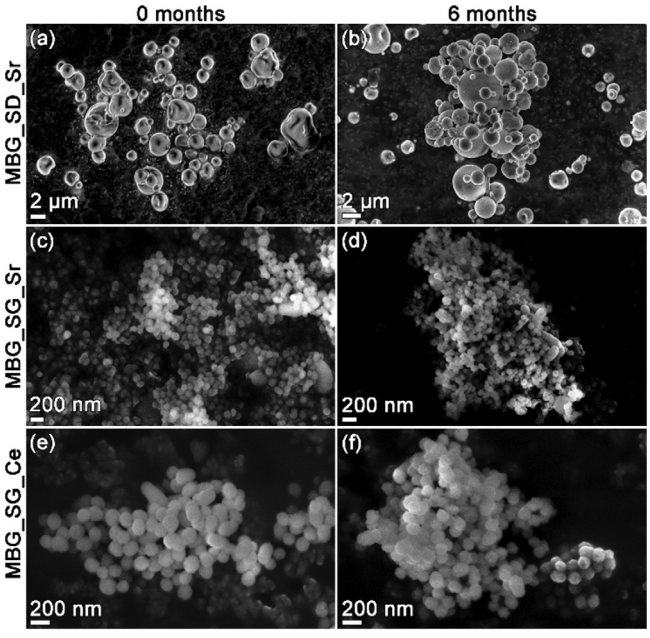

Fig. 2. SEM micrographs of (a,b) MBG_SD_Sr, (c, d) MBG_SG_Sr, and (e, f) MBG_SG_Ce prior to storage and after storage at accelerated conditions for six months.

materials have been proven non-cytotoxic and active in bone regeneration [3,7].

The stability of mesoporous glasses strongly depends on the synthesis procedure. It is observed that all MBGs decomposed rapidly in the accelerated storage conditions when they were calcined prior to storage. Both Sr-containing MBGs (MBG_SD_Sr and MBG_SG_Sr) show a rapid loss of specific surface area and total pore volume when stored at accelerated conditions without micelles in their pores, indicating that the pore system is collapsing when stored in a humid atmosphere. When stored in room conditions, the degradation of the MBG-SG_Sr is slower compared to MBG_SD_Sr, indicating a higher stability. Using spray-drying synthesis, the silica polymerization is promoted in a very short time-period compared to sol–gel synthesis, which results in a lower degree of silica condensation. The initial polymerization of silica species during the sol aging prior to spraying is a crucial step in the spray drying synthesis [44], and 1 h hydrolysis time of TEOS at pH 2 during the solution preparation does not allow for a high degree of silica crosslinking [45]. However, a too high condensation at this stage results in poor porosity of the material [46], making the hydrolysis time a delicate tradeoff.

It should also be noted that MBG_SD_Sr is synthesized with P123 as the surfactant, which produces a microporous network interconnecting the mesopores in comparison to MBG-SG_Sr, which is synthesized using CTAB and hence has a lower degree of microporosity (Fig. S1(b) and Fig. S3(b)). Galarneau et al. studied the stability of mesoporous silica synthesized with P123 and showed that the amount of microporosity affects the material degradation, where a high microporosity leads to a significant decrease in specific surface area and an increased mesopore size [47].

There is a clear difference in the stability of MBG_SD_Sr and MBG_SG_Sr stored with the micelles remaining in the pores. In MBG_SG_Sr, the CTAB is clearly stabilizing the material also during accelerated conditions. The spray dried material is degrading even though P123 remains in the pores in all storage conditions, indicating that the material degradation is not only rendered from humidity, but that the material is less stable. The large drop in specific surface area and pore volume for MBG_SD_Sr stored with micelles in accelerated conditions for three months is probably due to an insufficient sealing of the Eppendorf prior to storage allowing for a higher diffusion of humid air to and from the sample.

The difference in degradation rate between the sol–gel synthesized MBGs can be due to the addition of calcium nitrate tetrahydrate simultaneously to the TEOS addition (MBG_SG_Sr) or 30 min after TEOS addition (MBG_SG_Ce). The delayed addition time allows a higher degree of silica condensation prior to addition of calcium. It should also be noted that the therapeutic ion is added post-synthetically for MBG_SG_Ce. The Ce is added by mixing the precursor with ethanol and the calcined parent material, MBG_SG_Ce_Parent, which might affect the surface chemistry of the MBG. Also, the higher calcination temperature of MBG_SG_Ce (700 °C) compared to MBG_SG_Sr (600 °C) can contribute to the higher material stability.

SBA-15 mesoporous silica stored in Eppendorfs

Fig. 3 shows the evolution of the specific surface area and total pore volume for the mesoporous silica of SBA-15 type synthesized with various amounts of heptane and NH_4F. All SBA-15 samples appear stable upon storage at dry and room conditions, but at accelerated storage conditions SBA-15_2 and SBA-15_3 lose 27 % and 34 % of their specific surface area, respectively, when stored without micelles in the pores, whilst SBA-15_1 is more stable in all storage conditions.

The morphology of the mesoporous SBA-15 silicas before and after storage in accelerated conditions for six months is shown in

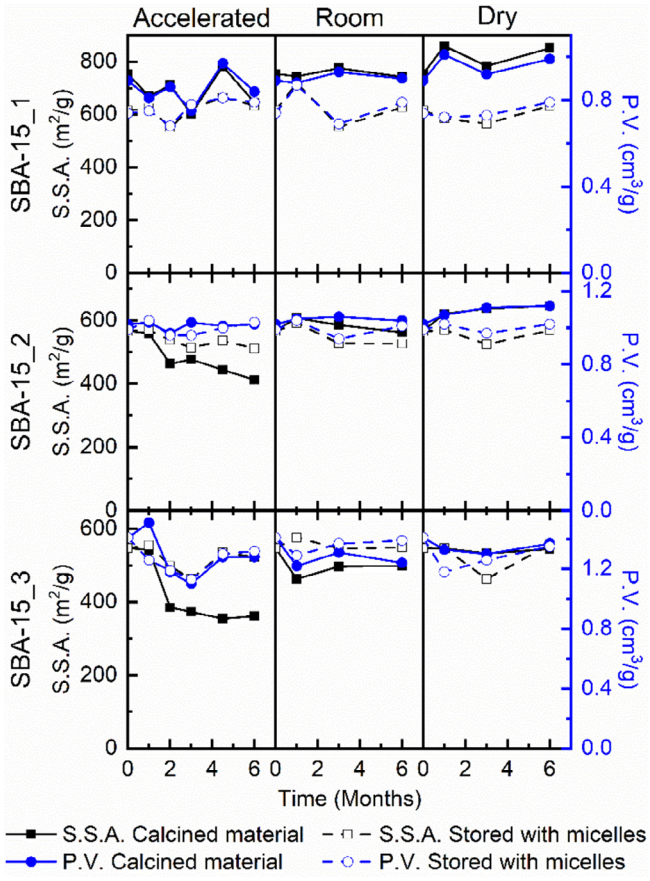

Fig. 3. Evolution of specific surface area and total pore volume for SBA-15_1, SBA-15_2, and SBA-15_3 synthesized with various amounts of heptane and NH_4F stored with and without micelles.

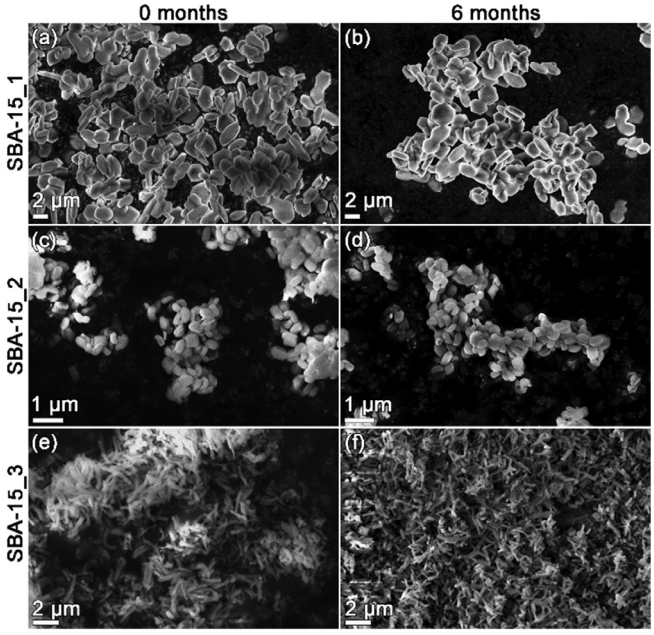

Fig. 4. SEM micrographs of (a, b) SBA-15_1, (c, d) SBA-15_2, and (e, f) SBA-15_3 prior to storage and after storage at accelerated conditions for six months.

Fig. 4. SBA-15_1 (Fig. 4(a, b)) has a 500 nm thick and ~2 μm wide platelet morphology, SBA-15_2 (Fig. 4(c, d)) consists of ~400 nm long and ~220 nm wide rods, and SBA-15_3 (Fig. 4(e, f)) comprises

~1000 nm long and ~260 nm wide rods. No morphological changes are observed upon storage.

Björk et al. reported that addition of heptane and NH_4F not only affect the particle morphology, but also the silica structure, i.e. linear vs cyclic silica species, changes in specific surface area and microporosity of the materials [18,48]. SBA-15 synthesized with no or low amounts of NH_4F, such as SBA-15_1, have a lower amount of six-fold cyclic species compared to SBA-15 materials synthesized with a higher salt concentration, such as SBA-15_2 and SBA-15_3 [48]. The decomposition at accelerated storage conditions corresponds well to the results from Broyer et al. [49], who showed that mesoporous silica of MCM-41 decomposes in humid environments.

It is apparent that the pure silicas are more stable compared to the MBGs. This is most probable due to a higher condensation of the silica framework as this is not disturbed by addition of Ca.

Further, it should be noted that the majority of the surface loss in these two materials occurs during the first two months of storage. This can be due to collapse of the microporous network in these materials (Fig. S9(b) and Fig. S11(b)). There is no notable decrease in the specific surface area and pore volume when the materials are stored prior to calcination, i.e. with the micelles in the pores. This shows that the micelles are supporting the structure and prevents the degradation of the micropores.

Mesoporous carbons stored in Eppendorfs

Fig. 5 shows that the long-time stability of mesoporous carbons in terms of specific surface area and pore volume is highly independent of the tested storage conditions. No material degradation can be observed even at accelerated conditions. Fig. 6 presents the morphology of CMK-1_Ag (Fig. 6(a, b)) that consists of ~120 nm large spheres, and CMK-3_Ag (Fig. 6(c, d)) comprises ~330 nm wide and ~900 nm long rods, before and after storage in accelerated conditions for six months. No morphological changes are observed. It is clear that the mesoporous carbons can be stored for a significant time without changes, most probably due to their hydrophobic properties.

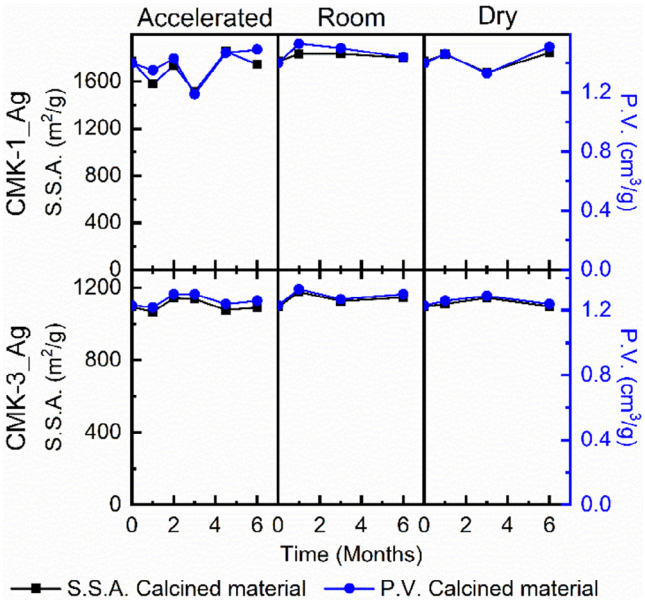

Fig. 5. Evolution of specific surface area and total pore volume for CMK-1_Ag and CMK-3_Ag.

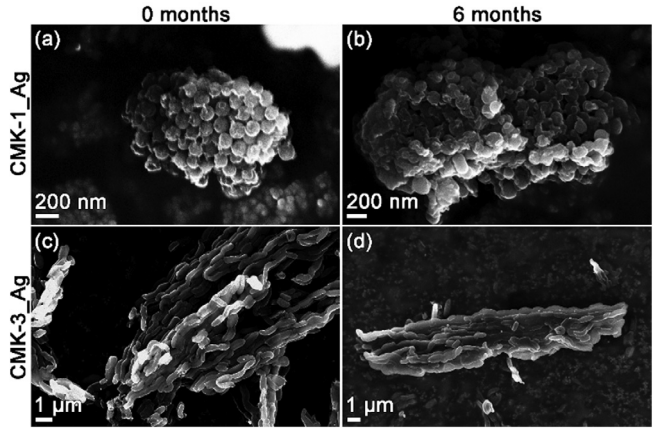

Fig. 6. SEM micrographs of (a, b) CMK-1_Ag, (c, d) CMK-3_Ag prior to storage and after storage at accelerated conditions for six months.

Storage in glass vials

Materials characteristics

To evaluate the effect of the storage container, two calcined bioactive glasses, MBG_SD_Sr and MBG_SG_Cu, were stored in glass vials under accelerated conditions for 2 months. The materials (both spray dried and sol–gel synthesized MBGs) showed low stability in Eppendorfs (Fig. 1), but excellent behavior in bone repair and wound healing, respectively [3,5,50]. Nitrogen physisorption isotherms and pore size distributions for the materials before and after storage are presented in Fig. 7(a, b) and Table 2. It can be observed that the specific surface area of the materials decreases by <10% compared to the surface loss of >90% when stored in Eppendorfs.

The SEM micrographs shown in Fig. 7(c–f) demonstrate that there is no morphological change during the storage. MBG_SG_Cu consists of 50–150 nm large particles, and MBG_SD_Sr comprises larger spheres in the size range of 0.5–5 µm. The material composition was determined using EDS, and the ion concentration is presented in Table 2. As can be seen, there is no elemental change in the materials during the storage.

Ion release profiles in TRIS for both materials were measured by ICP and are shown in Fig. 7(g, h). Both materials show a burst release with a high degree of ion release during the first 15 min in TRIS. The shape of the ion release profiles is not changing upon storage. There is however a slight shift in the values between the samples. This shift can be associated with the preparation of the samples prior to the ICP measurements, as the low amount of weighed MBG powder required to evaluate the ion release behavior could lead to an experimental error. The shift should not be regarded as a change in the material characteristics.

The increased stability in glass vials compared to Eppendorf shows the importance of storing the MBGs in a sealed container. The Eppendorf allows water vapor from the humid air to access the materials, even after sealing with parafilm (0.88 g/m^2/24 h (37.8 °C and 90% R.H. vs desiccant)) [51], which is not possible using a glass vial. As can be observed in Fig. 1, the samples stored in a dry atmosphere did not degrade during the 6 months storage, whilst under accelerated conditions, the materials lost their porosity and surface area within one month. When stored in glass vials, the materials are stable for at least two months under accelerated conditions, and therefore storage for at least six months in dry conditions should be possible, see Fig. 1 and Supplementary Information Table S1 and S3. The small loss observed in specific surface area and pore volume can be due to humidity in the air that is enclosed with the sample, as this was not performed in e.g. N_2

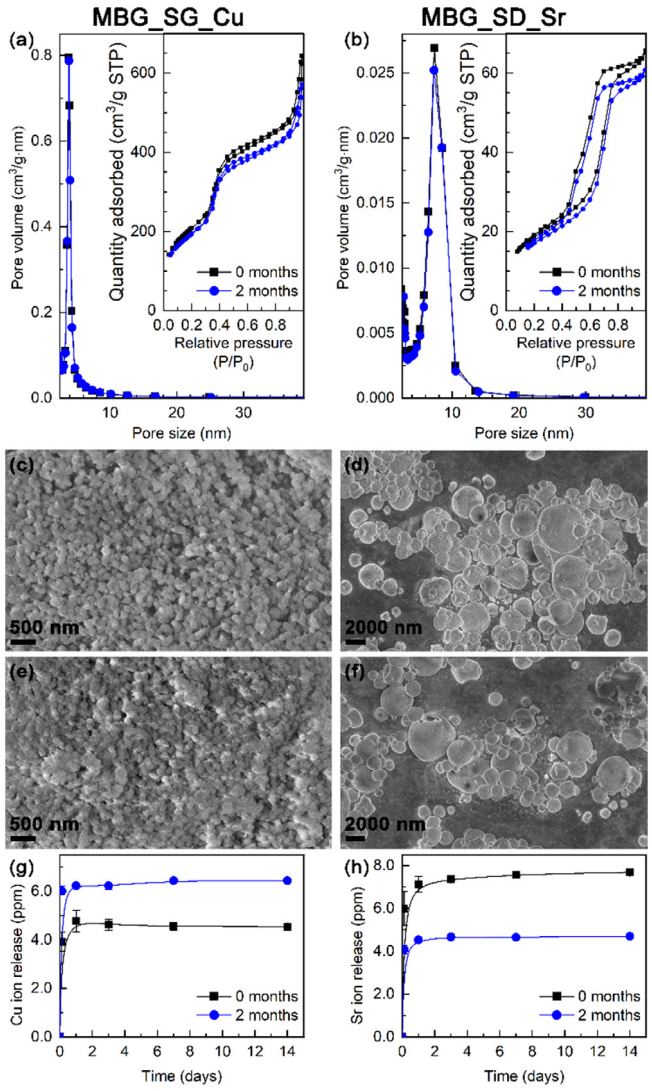

Fig. 7. Evolution of characteristics of calcined MBG_SG_Cu (left) and MBG_SD_Sr (right) particles stored in glass vials under accelerated conditions for two months: (a, b) nitrogen physisorption isotherms and pore size distributions, SEM micrographs of the materials (c, d) before storage and (e, f) after storage, and (g, h) ion release profiles for the respective materials.

atmosphere. A similar loss is observed for MBG_SD_Sr stored in dry conditions in Eppendorfs. From this we conclude that the materials, especially MBGs should be stored in containers where water vapor can not diffuse.

Sterility and cytotoxicity

Prior to the storage, the MBGs were sterilized using 25 kGy gamma radiation. The sterility of the materials was assessed by exposing *Staphylococcus epidermidis* in TSB solution to the selected MBGs. Bacterial growth was evaluated by studying the transparency of the solution. As can be observed in Fig. 8, both bioactive glasses are considered sterile both before and after the storage.

Cytotoxicity tests were performed following ISO 10993-5: 2009-Biological Evaluation of Medical Devices Tests for In vitro cytotoxicity. Fibroblast cells (L929) were used as a model cell line to test the cytotoxicity of the bioactive glasses. A polystyrene plate was used as a negative control and a polystyrene plate with 0.08 mg/mL of NPS to induce cell death was used as positive control. The standard defines cell viability above 70% as cytocompatible, and a reduction of cell viability by more than 30% is considered to be a cytotoxic effect.

Fig. 9 shows the cell viability for MBG_SD_Sr (concentration: 1 mg/mL) before and after storage. The OD data shows cell viability >70% both before and after storage and the material is hence considered to be cytocompatible. The lower cell viability at 0 months compared to 2 months is attributed to particle agglomeration which reduces the space on the polystyrene plate and results in a decreased cell viability.

Fig. 10 shows the cell viability for MBG_SG_Cu (concentration: 1 mg/mL) before and after storage. The OD data shows a cell viability $\leq$70% both before and after storage and the material is hence considered to be cytotoxic at this concentration. The dark spots in the optical micrograph for MBG-SG-Cu at 2 months show aggregation of particles which can induce a locally high, toxic, Cu concentration. An MTT assay was also performed on MBG_SG_Cu at a lower concentration (concentration: 0.2 mg/mL), and the results are shown in Fig. 11. At this concentration, the cell viability is >70%, and the material is not cytotoxic, neither before nor after storage. This clearly shows that the material concentration is crucial in biological applications, and that the biocompatibility is not affected by the storage.

Conclusions

This study shows the impact of storage conditions on various silica- and carbon-based mesoporous materials. The accelerated storage conditions provide a good view of the stability of the various materials. It is clear that bioactive glasses are more sensitive to humidity compared to SBA-15 mesoporous silica, and that mesoporous carbons of CMK-1 and CMK-3 types are unaffected by storage temperature and humidity. Humidity is the main factor for material degradation, resulting in that silica based materials should be stored in glass vials rather than Eppendorfs as this does not allow transfer of humidity. Storing materials prior to calcination, have a favourable effect on the storage as the micelles stabilize the material and reduces structural degradation. It should however be noted that this can be a challenge in a commercial perspective, as optimal storage would result in that the customer needs to calcine the material, which is not always suitable. The sterility and cytotoxicity of MBG materials stored in glass vials are not affected during storage in accelerated conditions for

Table 2
Physicochemical properties of the MBG materials stored in glass vials prior to and after storage under accelerated conditions for two months.

Sample	Storage time	Specific surface area (m^2/g)	Pore size (nm)	Pore volume (cm^3/g)	X^c/(X + Si) atomic %
MBG_SG_Cu	0 month	762	3.5	0.99	2.2 ± 0.6
	2 months	710	3.5	0.88	2.4 ± 0.6
MBG_SD_Sr	0 month	68	3.5	0.10	2.5 ± 0.3
	2 months	62	3.5	0.09	2.2 ± 0.2

[a] Calculated with the BET-method.
[b] Calculated with the BJH-method.
[c] X = Cu or Sr.

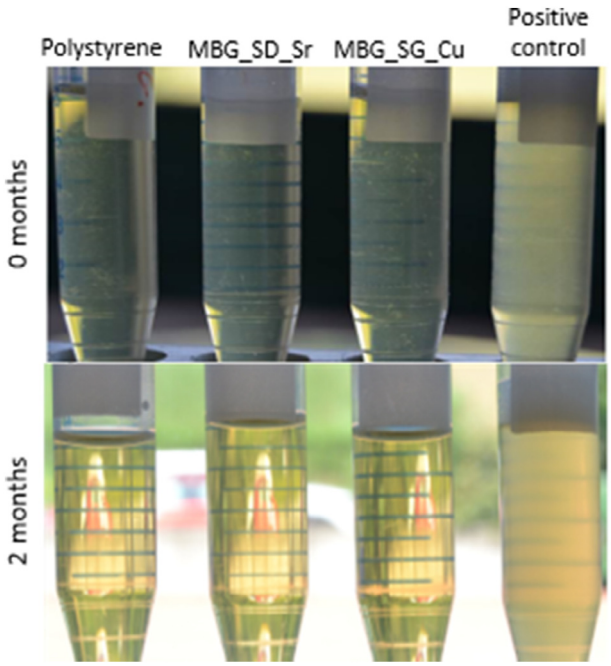

Fig. 8. Images from sterility tests of MBG_SG_Cu and MBG_SD_Sr. Bacteria growth is observed in the positive control through lack of transparency of the solution.

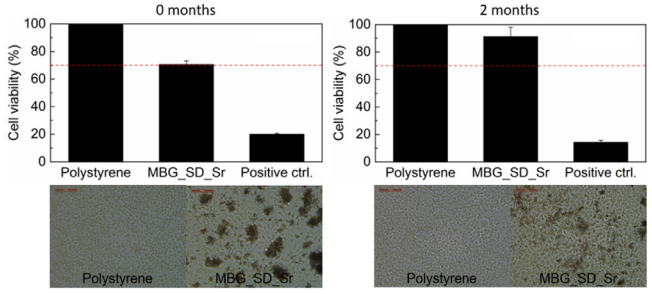

Fig. 9. Quantification of cell viability through MTT assay for MBG_SD_Sr (1 mg/mL) before and after storage for 2 months at accelerated conditions in glass vials compared to polystyrene (negative control) and polystyrene with 0.08 mg/mL of NPS (positive control). The red line at 70 % represents the limit for cytotoxicity. Below are optical images of cells after 72 h of incubation with MBG_SD_Sr at concentration of 1 mg/mL compared to the negative and positive control. (Scale bar 100 μm).

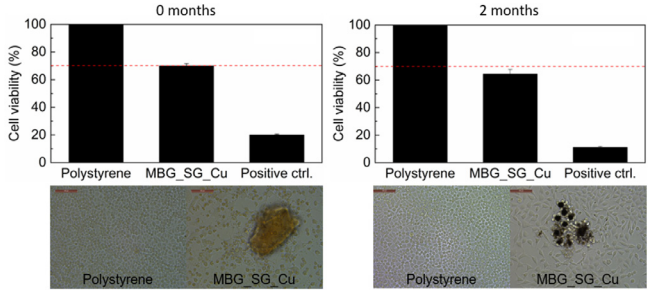

Fig. 10. Quantification of cell viability through MTT assay for MBG_SG_Cu (1 mg/mL) before and after storage for 2 months at accelerated conditions in glass vials compared to polystyrene (negative control) and polystyrene with 0.08 mg/mL of NPS (positive control). The red line at 70 % represents the limit for biocompatibility. Below are optical images of cells after 72 h of incubation with MBG_SG_Cu at concentration of 1 mg/mL compared to the negative and positive control. (Scale bar 100 μm.)

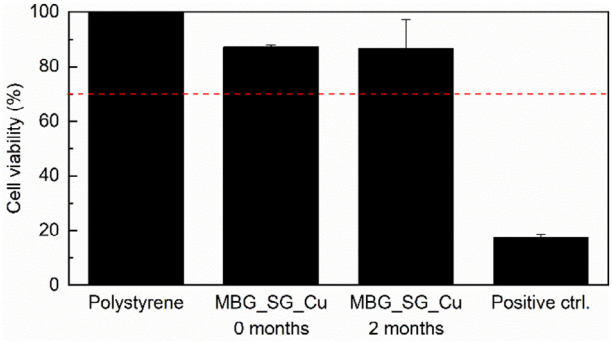

Fig. 11. Quantification of cell viability through MTT assay for MBG_SG_Cu (0.2 mg/mL) before and after storage for 2 months at accelerated conditions in glass vials compared to polystyrene (negative control) and polystyrene with 0.08 mg/mL of NPS (positive control). The red line at 70 % represents the limit for cytotoxicity.

2 months, which corresponds to >6 months of storage in dry conditions. The information in this study is of importance for commercialization of mesoporous silica- and carbon-based materials for medical applications, and we conclude that mesoporous silica-based materials should be stored dry, in containers that does not allow for water vapor diffusion, whilst mesoporous carbons can be stored in both dry and humid atmospheres.

Declaration of Competing Interest

The authors declare that they have no known competing financial interests or personal relationships that could have appeared to influence the work reported in this paper.

Acknowledgements

This project has received funding from the European Union's Horizon 2020 research and innovation programme under grant agreement No. 685872-MOZART (www.mozartproject.eu).

Appendix A. Supplementary data

Supplementary data to this article can be found online at https://doi.org/10.1016/j.jiec.2021.06.011.

References

[1] A. López-Noriega, D. Arcos, I. Izquierdo-Barba, Y. Sakamoto, O. Terasaki, M. Vallet-Regí, Chem. Mat. 18 (2006) 3137–3144.
[2] S. Kargozar, N. Lotfibakhshaeish, S. Ebrahimi-Barough, B. Nazari, R.G. Hill, Front. Bioeng. Biotechnol. 7 (2019) 355.
[3] S. Fiorilli, G. Molino, C. Pontremoli, G. Iviglia, E. Torre, C. Cassinelli, M. Morra, C. Vitale-Brovarone, Materials (Basel) 11 (2018) 678.
[4] K. Zheng, J. Kang, B. Rutkowski, M. Gawęda, J. Zhang, Y. Wang, N. Founier, M. Sitarz, N. Taccardi, A.R. Boccaccini, Front. Chem. 7 (2019).
[5] T.E. Paterson, A. Bari, A.J. Bullock, R. Turner, G. Montalbano, S. Fiorilli, C. Vitale-Brovarone, S. MacNeil, J. Shepherd, Front. Bioeng. Biotechnol. 8 (2020).
[6] S. Kargozar, M. Mozafari, S. Ghodrat, E. Fiume, F. Baino, Mater. Sci. Eng., C 121 (2021).
[7] K. Zheng, E. Torre, A. Bari, N. Taccardi, C. Cassinelli, M. Morra, S. Fiorilli, C. Vitale-Brovarone, G. Iviglia, A.R. Boccaccini, Mater. Today Bio 5 (2020).
[8] S. Kargozar, M. Mozafari, S. Hamzehlou, F. Baino, Front. Bioeng. Biotechnol. 7 (2019).
[9] L. Wang, W. Xu, Y. Chen, J. Wang, Sci. Rep. 9 (2019) 18175.
[10] C. Pontremoli, M. Boffito, S. Fiorilli, R. Laurano, A. Torchio, A. Bari, C. Tonda-Turo, G. Ciardelli, C. Vitale-Brovarone, Chem. Eng. J. 340 (2018) 103–113.
[11] L. Pontiroli, M. Dadkhah, G. Novajra, I. Tcacencu, S. Fiorilli, C. Vitale-Brovarone, Mater. Lett. 190 (2017) 111–114.
[12] Q. Liang, Q. Hu, G. Miao, B. Yuan, X. Chen, Mater. Lett. 148 (2015) 45–49.
[13] C. Wu, J. Chang, W. Fan, J. Mater. Chem. 22 (2012) 16801–16809.
[14] J.M. Rosenholm, V. Mamaeva, C. Sahlgren, M. Lindén, Nanomedicine 7 (2011) 111–120.
[15] M. Manzano, M. Vallet-Regí, Adv. Funct. Mater. 30 (2020) 1902634.

[16] H. Gustafsson, E.M. Johansson, A. Barrabino, M. Odén, K. Holmberg, Colloids Surf., B 100 (2012) 22–30.
[17] D. Sen Karaman, S. Sarwar, D. Desai, E.M. Björk, M. Odén, P. Chakrabarti, J.M. Rosenholm, S. Chakraborti, J. Mater. Chem. B, 4 (2016) 3292–3304.
[18] E.M. Björk, F. Söderlind, M. Odén, Langmuir 29 (2013) 13551–13561.
[19] S. Rostamnia, X. Liu, D. Zheng, J. Colloid Interface Sci. 432 (2014) 86–91.
[20] S. Rostamnia, T. Rahmani, H. Xin, J. Ind. Eng. Chem. 32 (2015) 218–224.
[21] A. Atakan, J. Keraudy, P. Makie, C. Hulteberg, E.M. Bjork, M. Oden, J. Colloid Interface Sci. 546 (2019) 163–173.
[22] S.-U. Lee, E.S. Kim, T.-W. Kim, J.-R. Kim, K.-E. Jeong, S. Lee, C.-U. Kim, J. Ind. Eng. Chem. 83 (2020) 366–374.
[23] A. Maleki, T. Kari, M. Aghaei, J. Porous Mat. 24 (2017) 1481–1496.
[24] S.H. Mansourian, S. Shahhosseini, A. Maleki, J. Ind. Eng. Chem. 80 (2019) 576–589.
[25] M.A. Isaacs, C.M.A. Parlett, N. Robinson, L.J. Durndell, J.C. Manayil, S.K. Beaumont, S. Jiang, N.S. Hondow, A.C. Lamb, D. Jampaiah, M.L. Johns, K. Wilson, A.F. Lee, Nat. Catal. 3 (2020) 921–931.
[26] F.S. Taheri, A. Ghaemi, A. Maleki, S. Shahhosseini, Energy Fuels 33 (2019) 5384–5397.
[27] X.N. Pham, M.B. Nguyen, H.S. Ngo, H.V. Doan, J. Ind. Eng. Chem. 90 (2020) 358–370.
[28] L. Paul, S. Mukherjee, S. Chatterjee, A. Bhaumik, D. Das, ACS Omega 4 (2019) 17857–17863.
[29] F. Zhang, X. Zheng, E. Liu, L. Yu, Y. Yan, J. Ind. Eng. Chem. 46 (2017) 397–403.
[30] Q. Zhao, Y. Lin, N. Han, X. Li, H. Geng, X. Wang, Y. Cui, S. Wang, Drug Delivery 24 (2017) 94–107.
[31] E. Torre, D. Giasafaki, T. Steriotis, C. Cassinelli, M. Morra, S. Fiorilli, C. Vitale-Brovarone, G. Charalambopoulou, G. Iviglia, Int. J. Nanomed. 14 (2019) 10147–10164.
[32] M. Gisbert-Garzarán, J.C. Berkmann, D. Giasafaki, D. Lozano, K. Spyrou, M. Manzano, T. Steriotis, G.N. Duda, K. Schmidt-Bleek, G. Charalambopoulou, M. Vallet-Regí, ACS Appl. Mater. Interfaces 12 (2020) 14946–14957.
[33] P.F.M. Menci, A. Charbonneau, C. Lefebvre, L.-P. De Nardo, Materials, 12 (2019).
[34] B. Adeniran, R. Mokaya, Chem. Mater. 24 (2012) 4450–4458.
[35] M. Boffito, C. Pontremoli, S. Fiorilli, R. Laurano, G. Ciardelli, C. Vitale-Brovarone, Pharmaceutics 11 (2019).
[36] D. Kozon, K. Zheng, E. Boccardi, Y. Liu, L. Liverani, A.R. Boccaccini, Materials (Basel) 9 (2016) 225.
[37] W. Stöber, A. Fink, E. Bohn, J. Colloid Interface Sci. 26 (1968) 62–69.
[38] T.W. Kim, P.W. Chung, I.I. Slowing, M. Tsunoda, E.S. Yeung, V.S.Y. Lin, Nano Lett. 8 (2008) 3724–3727.
[39] S. Jun, S.H. Joo, R. Ryoo, M. Kruk, M. Jaroniec, Z. Liu, T. Ohsuna, O. Terasaki, J. Am. Chem. Soc. 122 (2000) 10712–10713.
[40] V. Malgras, J. Tang, J. Wang, J. Kim, N.L. Torad, S. Dutta, K. Ariga, M.S.A. Hossain, Y. Yamauchi, K.C.W. Wu, J. Nanosci. Nanotechnol. 19 (2019) 3673–3685.
[41] D. Zhao, J. Feng, Q. Huo, N. Melosh, G.H. Fredrickson, B.F. Chmelka, G.D. Stucky, Science 279 (1998) 548–552.
[42] M. Shi, Z. Chen, S. Farnaghi, T. Friis, X. Mao, Y. Xiao, C. Wu, Acta Biomater. 30 (2016) 334–344.
[43] Y. Yamauchi, P. Gupta, K. Sato, N. Fukata, S.-I. Todoroki, S. Inoue, S. Kishimoto, J. Ceram. Soc. Jpn. 117 (2009) 198–202.
[44] C. Boissiere, D. Grosso, A. Chaumonnot, L. Nicole, C. Sanchez, Adv. Mater. 23 (2011) 599–623.
[45] K. Waldron, Z. Wu, W.D. Wu, W. Liu, D. Zhao, X.D. Chen, C. Selomulya, J. Mater. Chem. A 2 (2014) 19500–19508.
[46] C. Boissiere, D. Grosso, H. Amenitsch, A. Gibaud, A. Coupé, N. Baccile, C. Sanchez, Chem. Commun. (2003) 2798–2799.
[47] A. Galarneau, M. Nader, F. Guenneau, F. Di Renzo, A. Gedeon, J. Phys. Chem. C 111 (2007) 8268–8277.
[48] E.M. Björk, P. Mäkie, L. Rogström, A. Atakan, N. Schell, M. Odén, J. Colloid Interface Sci. 521 (2018) 183–189.
[49] M. Broyer, S. Valange, J.P. Bellat, O. Bertrand, G. Weber, Z. Gabelica, Langmuir 18 (2002) 5083–5091.
[50] A. Bari, N. Bloise, S. Fiorilli, G. Novajra, M. Vallet-Regí, G. Bruni, A. Torres-Pardo, J.M. González-Calbet, L. Visai, C. Vitale-Brovarone, Acta Biomater. 55 (2017) 493–504.
[51] https://www.sigmaaldrich.com/content/dam/sigma-aldrich/docs/Sigma/Product_Information_Sheet/1/p7668pis.pdf.